Opto-Electronic Science

CN 51-1800/O4 ISSN 2097-0382 (Print) ISSN 2097-4000 (Online)

Design, setup, and facilitation of the speckle structured illumination endoscopic system

Elizabeth Abraham and Zhaowei Liu

Citation: Abraham E, Liu ZW. Design, setup, and facilitation of the speckle structured illumination endoscopic system. *Opto-Electron Sci* **4**, 240022 (2025).

https://doi.org/10.29026/oes.2025.240022

Received: 4 August 2024; Accepted: 30 September 2024; Published online: 13 December 2024

Opto-Electronic Science

Article

March 2025, Vol. 4, No. 3

DOI: 10.29026/oes.2025.240022 CSTR: 32246.14.oes.2025.240022

Design, setup, and facilitation of the speckle structured illumination endoscopic system

Elizabeth Abraham and Zhaowei Liu*

Structured illumination, a wide-field imaging approach used in microscopy to enhance image resolution beyond the system's diffraction limits, is a well-studied technique that has gained significant traction over the last two decades. However, when translated to endoscopic systems, severe deformations of illumination patterns occur due to the large depth of field (DOF) and the 3D nature of the targets, introducing significant implementation challenges. Hence, this study explores a speckle-based system that best suits endoscopic practices to enhance image resolution by using random illumination patterns. The study presents a prototypic model of an endoscopic add-on, its design, and fabrication facilitated by using the speckle structured illumination endoscopic (SSIE) system. The imaging results of the SSIE are explained on a colon phantom model at different imaging planes with a wide field of view (FOV) and DOF. The obtained imaging metrics are elucidated and compared with state-of-the-art (SOA) high-resolution endoscopic techniques. Moreover, the potential for a clinical translation of the prototypic SSIE model is also explored in this work. The incorporation of the add-on and its subsequent results on the colon phantom model could potentially pave the way for its successful integration and use in futuristic clinical endoscopic trials.

Keywords: speckle imaging; endoscopic add-on; colon phantom; clinical translation

Abraham E, Liu ZW. Design, setup, and facilitation of the speckle structured illumination endoscopic system. *Opto-Electron Sci* **4**, 240022 (2025).

Introduction

Gastrointestinal (GI) endoscopy, a technique practiced across the globe for several decades, is a vital and important diagnostic procedure used to visualize, image, assess, and treat various conditions of the GI tract[1]. In the United States alone, it is estimated that more than 20 million GI endoscopies are performed annually[2–4]. Existing since the early 1800s in its primitive forms, white-light endoscopy (WLE) has played an integral role in the visualization and diagnosis of the GI, the evolution and use of which have greatly increased over the years. This trend is set to rise in the coming years[5–7]. Over the last few years, several imaging modalities have been developed to help facilitate the WLE process, capable of imaging both surface and subsurface planes. In all imaging applications, image quality is of critical importance, primarily determined by the image resolution, contrast, and noise[8]. High resolution enhances the ability to perceive details of an image, as opposed to solely using optical or digital magnification, which may not prove useful for a detail-oriented image screen and analysis. However, digital, or optical magnification, in conjunction with high-resolution imaging techniques, may help better visualize images. Therefore, the importance of high image resolution in endoscopy plays a vital role in its visual screening and diagnosis for an accurate identification of anomalies within the human body[9–11]. Hence, as a vital bridging metric, good image resolution in endoscopy is critical,

Department of Electrical and Computer Engineering, University of California, San Diego, 9500 Gilman Drive, La Jolla, California 92093, United States.

*Correspondence: ZW Liu, E-mail: zhaowei@ucsd.edu

Received: 4 August 2024; Accepted: 30 September 2024; Published online: 13 December 2024

warranting a need for its study, integration, and usage.

Imaging techniques in endoscopy where resolution plays a critical role has made significant strides in the last decade wherein, several advances in WLE under both hardware and software realms have proven to be significantly useful in detecting mucosal and other bodily abnormalities[12–20]. However, as observed from these state-of-the-art (SOA) technologies, the resolution levels, field of view (FOV), and the depth of field (DOF) are jointly restricted and typically capped to an extent determined by their software and hardware capabilities. In comparison, the speckle structured illumination endoscopy (SSIE) imaging approach is capable of circumventing these limitations, opening up new opportunities as explained in our previous works[21]. Concisely, SSIE obtains its enhanced resolution at wide FOV and DOF by employing high-resolution illumination speckles and an efficient image reconstruction algorithm, namely blind-structured illumination microscopy (SIM), using multiple low-resolution frames. The speckles produced in the SSIE system result from the random interference of laser illumination originating from the two multimode (MM) fibers placed on either end of the endoscope. The two-fiber interference model used in SSIE, the reasoning behind it, and the characterization of the system and its working principles were explained in our previous study[21].

As an extension of our previous work, this study mainly explores the prototypic design and model of the add-on developed, the integrated setup of the SSIE, its performance, and facilitation on a colon phantom model, with the view for its potential translation into futuristic clinical explorations. Furthermore, as SSIE employs N frames of low-resolution images to achieve a single frame high-resolution image via the blind-SIM algorithm, we examine the effect of the number of frames N on the achievable resolution enhancement at various image distances. SSIE may be used to complement standard WLE practices at optimal parameters for enhanced screening, visualization, and assessment of images at high levels of resolution, along with its wide FOV and DOF, cost-effectiveness, ease of integration, and use. The remainder of the paper is structured as follows: the first section explores the different bench top components of the SSIE, the second section describes a low-cost design of an external sleeve to hold the fibers around the endoscope for illumination. In addition, this section also discusses other design considerations of the prototypic add-on and its potential clinical translation. The third section explores the fabrication of the colon phantom, followed by the fourth section showing the experimental results obtained from it and relevant analysis. Lastly, the study ends with a discussion and conclusion section encompassing the future prospects.

SSIE setup and experimental results

The schematic of the SSIE is illustrated in Fig.1. The SSIE

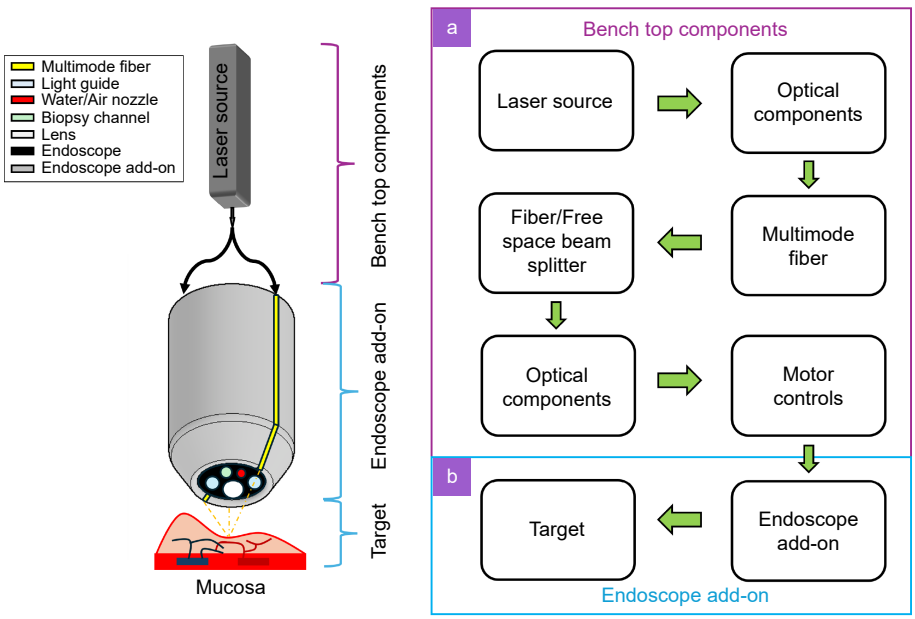

Fig. 1 | Schematic of the SSIE system. (**a**) Bench top components. Block 1: laser source of 532 nm; Block 2 (optical components): optical mirrors; Block 3: MM fiber; Block 4: fiber/free space beam splitter; Block 5 (optical components): collimators, optical mirrors and MM fiber; Block 6: step motor, processor, and motor controls. (**b**) Endoscope add-on (right to left). Block 7: endoscopic add-on; Block 8: target (colon phantom model).

can be broadly classified into two categories, namely the benchtop components and the endoscopic add-on.

Bench top components

The experimental setup of the SSIE (Fig. 1) is illustrated in Fig. 2 and Fig. 3. In the SSIE system, a laser source of a known wavelength is directed through blocks 1 to 6 (Fig. 1) via two MM fibers and onto the target through block 7 (Fig. 1), the endoscopic add-on. The speckle patterns are modulated between image acquisition, following the blind-SIM principle[21]. The speckle pattern themselves do not affect the endoscopic imaging[21]. Additionally, the basic theory of speckle imaging and the mathematical model can be found in our previous study[21]. The illumination patterns originating from the two MM fibers placed at an angle on either end of the endoscope (Fig. 3) interfere at the target, causing spatial frequency mixing between the target and the incident illumination patterns. This spatial mixing encodes structural details corresponding to the high spatial frequency details of the target into detectable low spatial frequency information. Hence, high-frequency components of the target, which are lost by conventional imaging techniques, can be effectively recovered. To facilitate a super-resolution image of SIM, an image reconstruction algorithm utilizes a series of such low-resolution images with different illumination patterns captured by the endoscopic charge-coupled device (CCD)[22–26]. Blocks 1 to 5 of Fig. 1 are illustrated in Fig. 2.

The fiber and free-space setup (Fig. 1(a, b)) essentially performs the same functionality, which is to route an external visible laser source with a wavelength of 532 nanometers (used in this study) into the two MM fibers. These fibers are wound around the endoscopic probe in a particular fashion (see Supplementary information Section 1). Although both setups serve the same purpose, the fiber-based setup is more likely to have firm interconnections and be portable due to its compact size. Additionally, it is comparatively more robust against possible mechanical movements, whether large or small, compared to its free-space counterpart. However, in both setups, regardless of the type, the system's performance largely depends on the coupling efficiency of the laser beam into the MM fibers and the efficiency of the laser source itself. In the fiber-based setup, the external laser source is routed through mirrors, a fiber launch, and into the 50/50 fiber beam splitter, which is coupled to connectors 1 and 2. These connectors are attached to two MM fibers wound around the endoscope to deliver the laser illumination onto the sample. In the free-space setup, the fiber beam splitter is replaced with a free-space beam splitter, a mirror, and two external collimators. The MM fibers are routed onto a step motor programmed to provide vibration to the MM fiber, aiding in the modulation of the illumination patterns between successive frame acquisitions. The vibration of the fiber

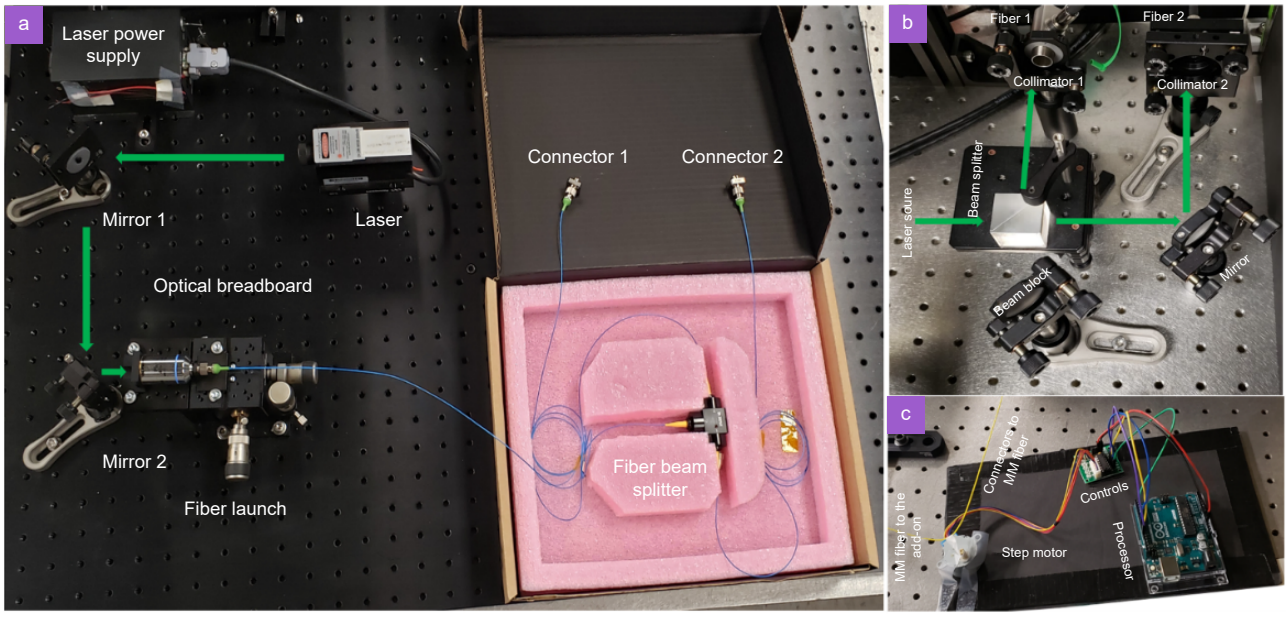

Fig. 2 | Experimental SSIE benchtop setup. (**a**) Fiber based setup. (**b**) Free space setup. The arrow denotes the pathway and direction of the laser beams traversal. (**c**) Step motor programmed to aid in the MM fiber modulation.

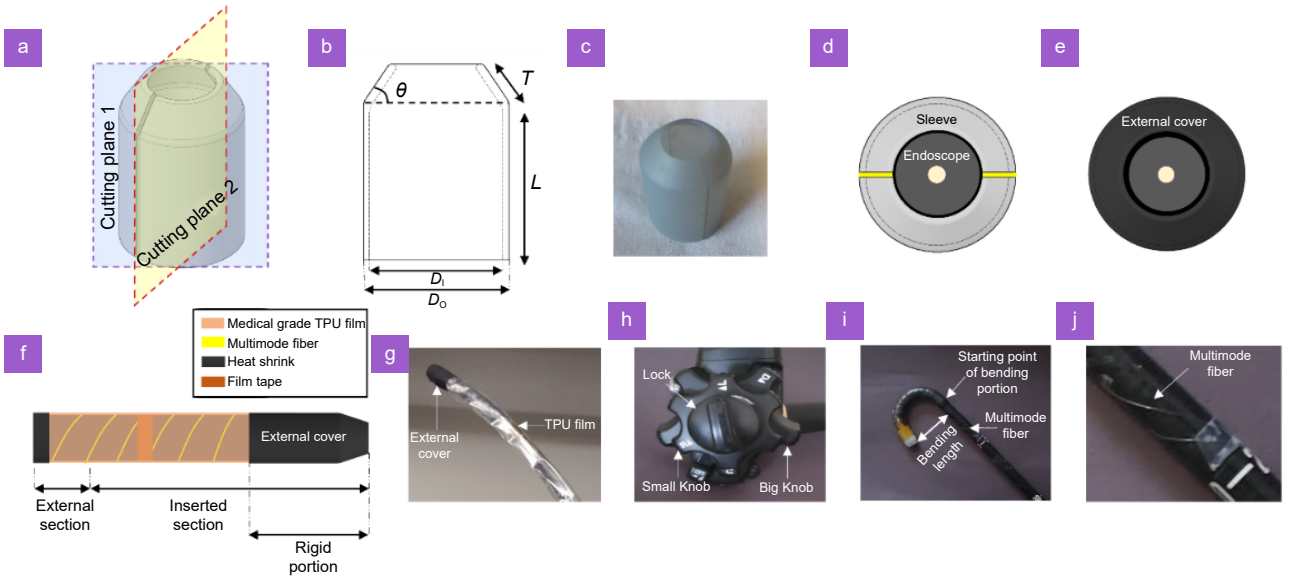

Fig. 3 | Design and fabrication of the add-on sleeve. (**a**) 3D CAD (computer aided design) representation of the add-on sleeve with two fiber holding slits on either ends. (**b**) 2D model of the sleeve, cross section of (a) along cutting plane 1, D_I and D_O are the internal and outer diameters, L is the length of the sleeve, T represents the tilt length and θ represents the tilt angle. The cross sections are identical across cutting planes 1 and 2. (**c**) Photograph of the 3D printed sleeve. (**d**, **e**) Schematic of the cross-sectional front end of the endoscope probe without and with the external cover (heat shrink tape) (yellow color slits on either ends represent the fiber slits), respectively. (**f**) Schematic of the side view of the endoscopic probe with different layers. The inserted portion refers to the section potentially put into the human body/region of examination and the external portion refers to the rest of the endoscopic probe which is connected to the laser setup of the SSIE (Fig.1(a, b)). (**g**) Photograph of an example Olympus CV-160 endoscopic probe with the sleeve (grey color) which is placed inside an external cover made of heat shrink tape (black) along with the TPU film. (**h**) Control knobs of the endoscopic probe. (**i**) Picture to depict the bending length of the endoscopic probe with the add-on sleeve (grey color) attached to the endoscope tip (rigid portion: head). (**j**) Magnified image of the MM fiber wound around the endoscope insertion tube.

introduces random phase, modifying the speckle pattern. The step motor is programmed to vibrate once every few milliseconds, but it can be programmed at a higher frequency through software, depending on experimental needs.

Design and fabrication of the add-on

In order to accommodate the two external MM fibers that are wound around the endoscopic probe and hold the MM fibers at an appropriate angle to illuminate the target, an external sleeve is designed to facilitate this (Fig. 3).

To accommodate the large DOF typically allowed by a wide-angle lens endoscope (WLE), the add-on must be designed to assist in imaging at different planes if needed. The sleeve design in Fig. 3(a, b) is designed in a manner wherein the tilt angle (θ) and the tilt length (T) can be modified as needed in the computer-aided design (CAD) file to capture samples at different imaging planes. However, as noted in our prior findings, the closer the sample plane is to the endoscopic detector, the higher the image resolution enhancement[21]. This is because the closer the sample or object plane is to the endoscopic detector, the larger the angle of interference of the laser illumination beams originating from the two multimode (MM) fibers placed on either end of the endoscopic probe. The larger the angle of interference, the higher the resolution of the speckle patterns. Since over the years, many versions of WLEs have been manufactured with varying diameters and lengths of the rigid portion (L) (Fig. 3(b)), the design parameters of the add-on, namely, the internal and external diameters (D_I, D_O), tilt angle (θ), tilt length (T), and the length of the rigid portion of the endoscopic probe (L), can be adapted accordingly as needed.

The design parameters for the fabricated sleeve in Fig. 3 are presented in Table 1. The parameters that contribute to the structural integrity and overall completeness of the sleeve consist of its physical dimensions, particularly the thickness, the materials used, the inherent CAD design of the sleeve, and the fastening of the external MM fibers as shown in Fig. 3(f) onto the distal tip of

Table 1 | Design and 3D printer parameters of the sleeve.

Design parameters	Values
Internal diameter (D_I)	10 mm
Outer diameter (D_O)	11.4 mm
Length (L)	2 cm
Tilt length (T)	3 mm
Tilt angle (θ)	75° to < 90° (for WD chosen in this study)
Fiber slit thickness	640 μm

the endoscope. Considering the dimensions of the MM fiber thickness and the capabilities of the 3D printer, a wall thickness of 0.7 millimeters, roughly three times the dimension of the MM fiber, is chosen. This thickness is selected to accommodate the fibers without compromising the structural strength and integrity of the add-on, especially during rigorous navigation protocols of the endoscope (refer to Supplementary information Section 2). Considering practical factors, the add-on is made with Grey pro resin due to its good structural strength, high precision, and resistance to heat and other deformations. For clinical prototypes, biocompatible and certified 3D resins with rigid and resistant properties may be utilized[27]. An alternative replacement for the resin sleeve material is ultra-thin glass (refer to Supplementary information Section 2). The CAD design of the sleeve inherently avoids sharp, rough, or uneven edges and corners. For clinical practices, standard post-processing measures such as washing, curing, and sanding, commonly used with biocompatible 3D printing materials, may be applied if and when necessary[28].

To cover the endoscopic probe (body), a medically approved polyether thermoplastic polyurethane (TPU) film is used to go over the MM fibers wound around the endoscope, as shown in Fig. 3(f). Polyether TPU is preferred due to its resistance to hydrolysis, skin oil, and microbes. Additionally, polyether TPU maintains good flexibility compared to ester-based TPUs, which is especially beneficial for endoscopic practices[29–30]. The TPU film can be heat-sealed or adjusted based on the dimensions of the endoscopic probe, or custom obtained from the manufacturer to fit the required dimensions of the endoscope. To cover the add-on, a polyolefin heat shrink with ultra-thin walls is utilized, as depicted in Fig. 3(g). Polyolefin is preferred due to its flexibility, durability, heat resistance, non-toxic nature, and ability to withstand most types of chemical corrosion[31–33]. Moreover, the polyolefin used in this study has relatively low heat shrink temperatures, approximately 2.5 to 5 times lower than the heat bearing capability of a standard endoscope, ensuring safe usage. Due to its low heat shrink temperatures, the underlying endoscopic body, typically made of thermoplastic polyester elastomer (TPC), thermoplastic polyurethane elastomer (TPU), and, in some cases, PVC material, is well preserved. The heat shrink (polyolefin) provides excellent coverage for the MM fibers secured along the fiber slits of the add-on. In a futuristic clinical system, the tips of the fibers may be blocked by food, water, or body fluid molecules, which can affect the flow of optical illumination onto the target. This is where the use of microtubing becomes useful, as presented in the Supplementary information Section 3 with an abstract design.

The bending length of the endoscopic probe, as shown in Fig. 3(i) is operated by the big and small control knobs in Fig. 3(h), is approximately 7 and 5 centimeters, respectively. The lock primarily controls and secures the scope in place during image acquisition. The MM fibers used in the study have short- and long-term bend radii of 1.5 and 3 centimeters, which are within the limits of the bending length of the endoscope to maintain structural integrity. Furthermore, the winding mechanism of the MM fibers also plays a critical role in the structural integrity of the SSIE (refer to Supplementary information Table 1). The design parameters used in Fig. 3 are summarized in Table 1 (refer to Supplementary information on the tilt angle: Section 4). The material and dimension considerations discussed in this study would be applicable universally, as most WLEs are made of similar polymer-based materials with analogous flexibility. The thickness of the materials and their sterilization protocols are crucial to ensure safe navigation of the endoscope (see Supplementary information Section 2). Considering the diameters of the colon and esophagus in the human body, the add-on is unlikely to affect the maneuverability of the endoscope[34]. The WLE used in Fig. 3 has an D_I of 10 mm (Table 1), however, irrespective of the scope's diameter being narrow or wide or despite the scope's application being industrial or clinical or it being

flexible or rigid, the sleeve dimensions can be modulated accordingly, facilitating the straightforward translation of the prototypic model to other scope's to perform the unanimous operation of imaging at optimal imaging metrics.

After the sleeve design is completed, the CAD model is sent to a 3D printer (Form 3+). The printer utilizes the low force stereolithography (SLA) fabrication method to manufacture the sleeve using the resin specified in this study. The low-force SLA method involves solidifying the liquid resin through linear laser illumination and a flexible resin tank, which reduces print forces and improves the reliability of the fabricated sleeve. Next, the device assembly takes place, where the components described above, as shown in Fig. 3(f), are physically assembled.

Experimental results

The designed and fabricated sleeve for the SSIE system aims to achieve high-resolution imaging, wide FOV, and large DOF for fine features on the colon phantom. A colon phantom with fine fluorescent features is constructed (refer to Fig. 4 and Supplementary information Section 5 for more details). Using this constructed colon phantom, the incoherent fluorescence imaging potential of SSIE is explored and demonstrated in this session, focusing on enhancing resolution at optimal parameters. Given that endoscopes have a wide FOV and large DOF, several imaging distances are selected to examine the robustness of the SSIE system across different planes, categorized as near, middle, and far imaging planes. Based on our previous work, we have estimated the expected amount of resolution enhancement for specific focal planes[21]. Figure 5 displays the imaging results obtained at

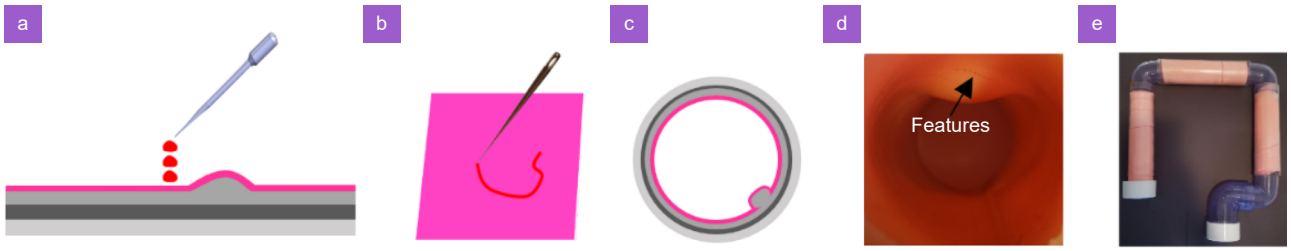

Fig. 4 | Phantom construction and feature deposition. (**a**) Schematic of feature deposition by drop casting fluorescence dye on sample. (**b**) Schematic of feature blood vessel drawing on silicone pads. (**c**) Schematic of the cross-sectional view of the colon model with bumps to simulate a realistic colon. (**d**) Photograph of the internal cross-sectional view of the colon phantom tunnel simulated with bumps where features drop cast and drawn. (**e**) Photograph of the external frame of the colon phantom.

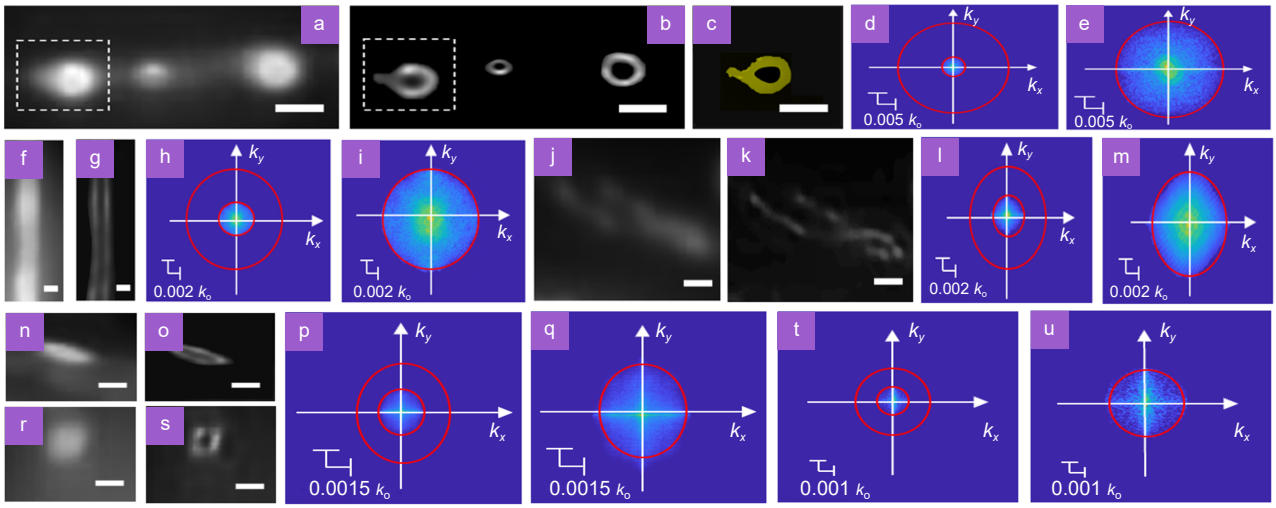

Fig. 5 | Fluorescence imaging results with SSIE on colon phantom. (**a**, **b**) Diffraction limited and enhanced SSIE image at imaging distance 2.7 cm. Scale bar: 200 μm. (**c**) Ground truth microscopic image of boxed region in (a). (**d**, **e**) Fourier spectra of (a) and (b). (**f**, **g**, **j**, **k**) Diffraction limited and enhanced SSIE image at imaging distance 5.7 cm. Scale bar: 2100 μm (large FOV: f, g), Scale bar: 800 μm (medium FOV: j, k). (**h**, **i**, **l**, **m**) Fourier spectra of (f, g, j, k). (**n**, **o**) Diffraction limited and enhanced SSIE image at imaging distance 7.2 cm. Scale bar: 500 μm. (**p**, **q**) Fourier spectra of (n) and (o). (**r**, **s**) Diffraction limited and enhanced SSIE image at imaging distance 10 cm. Scale bar: 400 μm. (**t**, **u**) Fourier transforms of (r) and (s).

different working or imaging distances (WD). The placement of the MM fibers is vertical, resulting in the vertical Fourier transform (FT) cutoff and slightly higher resolution enhancement vertically, as observed in Fig. 5.

The resolution enhancement of the SSIE system is assessed through the Fourier spectra plots of the diffraction-limited and enhanced images as shown in Fig. 5. A total of 150 samples are taken for SSIE processing. The DOF of samples in Fig. 5, 6 at different imaging planes range between 1–7 mm; however, this can be extended to as large as the WLE allows[21]. The resolving capacity and sharpness of edges in the SSIE images gradually decrease with the imaging distance (WD), consistent with the theoretical estimates of SSIE. However, the desired enhancement is maintained at a specific WD both visually (Fig. 5) and quantitatively (Table 2). In addition to resolving drop-cast features, the SSIE system is capable of imaging blood vessel-shaped line patterns to delineate, resolve, and enhance vessels at a wider FOV. Vessel-like structures on the mucosal or epidermal surface are often spread over a relatively large area, making them challenging to distinguish with a WLE probe. However, the enhanced SSIE images, compared to the diffraction-limited image, successfully resolve these non-distinguishable features, as observed in Fig. 5. The edges and borders of the vessels are well resolved over a wide FOV of 1.5 cm, as seen in Fig. 5(f). Even tangled or jointed globules of vessel features, as seen in Fig. 5(j), are fairly resolved in the processed frame (Fig. 5(k)). It should be noted that, as demonstrated in our previous works, imaging at closer WD can further enhance the image resolution at optimal metrics[21].

The quantitative experimental results, depicted in Table 2, align well with the theoretical estimations, despite the large coverage of DOF and FOV. The mathematical model behind this evaluation can be found in our prior study[21]. Furthermore, for a thorough analysis of image quality apart from image resolution, DOF, FOV, the qualitative metrics for Fig. 5 and Fig. 6 is also explored in the Supplementary information Section 9. In future systems, the WD can be reduced depending on the endoscopic optics, which would also result in a reduction in FOV. However, the advantage of the SSIE system is that resolution enhancement remains almost consistent across the entire FOV and can be extended to the extent allowed by a standard WLE. When comparing to other existing high-resolution methods, the SSIE method achieves good resolution with an optimal FOV and DOF, while maintaining hardware simplicity. In contrast, other compared systems rely on magnification and other physical design modifications in the imaging optics (refer to Section 6 in the Supplementary information for a

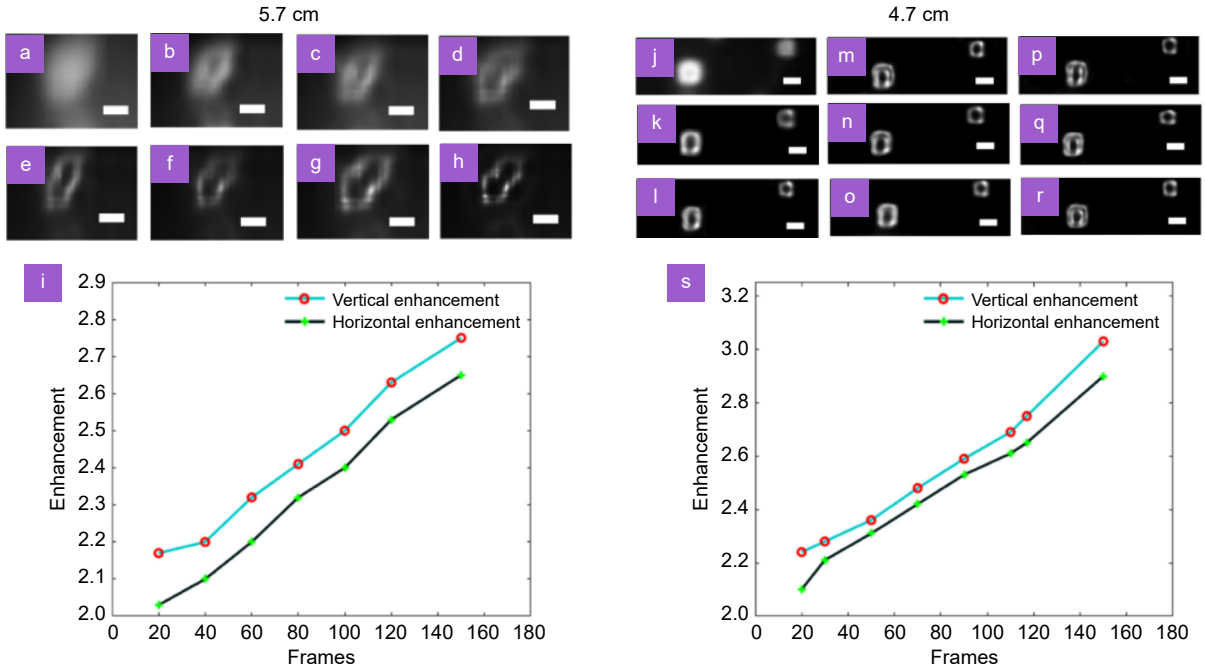

Fig. 6 | Sampling parameter vs enhancement. (**a**) Diffraction limited image. (**b–h**) Number of frames taken for SSIE processing: 20, 40, 60, 80, 100, 120, 150. Imaging distance: 5.7 cm, Scale bar: 200 μm. (**j**) Diffraction limited image. (**k–r**) Number of frames taken for SSIE processing: 20, 30, 50, 70, 90, 100, 110, 117, 150. Imaging distance: 4.7 cm, Scale bar: 600 μm. (**i**) Enhancement plot of (b–h). (**s**) Enhancement plot of (k–r).

Table 2 | Expected vs obtained resolution enhancement factor comparison.

Imaging distance	2.7 cm		5.7 cm		7.2 cm		10 cm	
	Vertical	Horizontal	Vertical	Horizontal	Vertical	Horizontal	Vertical	Horizontal
Expected	4.00	3.90	2.83	2.72	2.53	2.41	2.29	2.23
Obtained (Fig.5)	3.91 (b)	3.79 (b)	2.80 (g) 2.68 (k)	2.60 (g) 2.43 (k)	2.51 (p)	2.39 (p)	2.23 (t)	2.20 (t)

generic comparison of methods). The SSIE's coverage of a large FOV and DOF enables faster surface screening and visualization of samples compared to the state-of-the-art approaches. As part of our future work, the imaging speed of the SSIE can be further optimized[21]. From a clinical perspective, the potential improvement in *in vivo* imaging in humans is substantial when high spatial resolution is coupled with increased DOF and FOV.

The enhanced visualization of vessel-like structures on the phantom through the speckle phenomenon showcases the robustness and potential of the incoherent imaging SSIE modality with a wide FOV and DOF. While the enhancements are optimal and comparable with high accuracy, achieving a large FOV requires careful angling of the MM fibers, positioned along the vertical axis of the scope, to ensure that the specular illuminations originating from them cover the entire sample FOV. To achieve this, the two MM fibers placed on the axial ends of the endoscope must be centered towards the central axis of the endoscope[21].

In the previous SSIE demonstrations, we utilized a fixed number of frames, specifically 150 frames, for super-resolution image reconstruction. Now, we will examine the relationship between the number of frames and resolution enhancement. The summarized results are presented in Fig. 6. From the imaging results shown in Fig. 6, a phenomenological relation can be derived between the resolution enhancement factor and the number of sampling frames (N). The maximum enhancement is achieved with 150 frames (N) at an acquisition rate of 1 frame per second, as shown in Fig. 6. Obviously, decreasing the number of frames N results in a reduction of resolution enhancement. On average, a reduction of 0.1 times in overall image enhancement, both vertically and horizontally, is observed for a frame count reduction of 20. The plots in Fig. 6 display a linear decrement in resolution enhancement relative to the number of frames. It is worth noting that reducing the number of frames by almost half does not significantly affect image resolution enhancement. However, further reductions may have an impact on resolution enhancement, as observed in Fig. 6(i, s). The results in Fig. 6 indicate a linear relationship between enhancement and the number of frames, which is evident from the plots in Fig. 6(i, s). The linear relationship shown in Fig. 6 demonstrates that even with frame counts of 20 and 40, a small amount of image resolution enhancement of about 2 to 2.2 times is still possible. However, for the best results, each speckle pattern on the frames must be distinct from the others. From an information theory perspective, a minimum of N^2 subframes is required to reconstruct a super-resolution image with N-fold resolution improvement. Traditional structured illumination microscopy (SIM) utilizes sinusoidal patterns to efficiently sample the object, allowing for a small oversampling factor, denoted by α, where the total number of subframes is approximately αN^2 and α is close to 1. In contrast, speckle-based blind-SIM requires more frames, i.e., $\alpha > 1$, due to the lack of knowledge about the exact illumination patterns and the correlations between them (refer to Supplementary information for the flow of the blind-SIM process: Section 10).

Through experimentation, it has been determined that the oversampling factor α is around 12 for achieving the highest resolution enhancement, and less than 9 when reducing the number of frames by half from N. By selecting a reasonable α value, speckle-based blind-SIM demonstrates robustness and can achieve high levels of resolution enhancement[35]. Therefore, it is reasonable to expect, as shown in Fig. 6, that a reduction in the number of frames would result in seemingly less information about the exact illumination patterns and their correlations, leading to a decrease in resolution enhancement. This trend, explored through experimental results (Fig. 6), exhibits a seemingly linear behavior. The nature of the gradual slope and the correlations between frames will be further investigated in future studies[36]. Additionally, the intensity changes in Figs. 5, 6 is due to the nature of the imaging target and does not affect the imaging capabilities of the SSIE given N frames are cumulated for analysis. Further optimizations and directions for anincoherentclinicalstudyispresentedintheSupplementary information to be explored in our future efforts. The

combination of high resolution, wide FOV, large DOF, and high imaging speeds offered by SSIE may create new opportunities for clinical screening, imaging, and visualization. Additionally, the simplicity in design, implementation, and the low cost of SSIE make it suitable for translation into clinics, especially in resource-poor settings. Currently, the SSIE system takes approximately 2 to 3 minutes for image processing, but this can be optimized by employing faster GPU systems. Furthermore, the imaging speed of the SSIE can be enhanced by utilizing high-speed spatial light modulators (SLMs) to control the speckle patterns[21].

Discussion

The SSIE system, demonstrated in this study, serves as a low-cost, simplistic, non-invasive incoherent imaging endoscopic system that enhances high-resolution imaging with wide FOV and large DOF, complementing the standard WLE process. The straightforward design and robust optical imaging approach, as observed from the experimental results, make it applicable to various endoscopic models, whether for clinical or industrial use, with similar resolution improvement factors. Its simplicity and robustness enable its potential use in areas with limited infrastructure and resources. Furthermore, as a non-invasive visualization technique, the enhanced imaging capabilities of SSIE, particularly in capturing minute vessels and tissues, may allow clinicians to thoroughly inspect surface mucosa and potentially diagnose and treat abnormal epithelium and tissues of the GI tract. This study successfully applies the well-established concept of speckle imaging to endoscopy through the prototypic design developed, resulting in enhanced image resolution at optimal metrics[21]. While this study focuses on incoherent imaging, there is potential for its extension to scatter-based imaging, which requires further exploration in future efforts. We also intend to explore the incorporation of the add-on into endoscope subcomponents such as endocuffs and endorings to in our future efforts to facilitate the SSIE's imaging capabilities in addition to the scope's[37]. A prescreen of the design of endocuffs and endorings suggest, the MM fibers of the SSIE model can be adhered to them facilitating the SSIE imaging, although a thorough analysis remains to be explored in our future efforts. However, the imaging capabilities of the SSIE would remain similar and would only aim to aid and enhance the existing imaging capabilities of the endocuffs and endorings. In terms of image speed, the SSIE's current implementation captures 1 frame per second, taking around 4 minutes to capture 150 frames. However, newer scope models may offer faster image acquisition rates. Additionally, for fluorescent imaging, further optimizations can be explored in future studies[38–40] (see Supplementary information Section 7). Achieving real-time implementation of SSIE would require optimization from both hardware and software perspectives. Hardware-wise, the imaging speed can be increased by employing a spatial light modulator (SLM) with prior knowledge of the illumination patterns[21]. From a software perspective, the current processing time using a GTX 1080Ti graphics card and i7-8700k CPU is about 2–3 minutes. However, with the GeForce RTX 3090 Ti GPU, which offers higher clock frequency and bandwidth, the processing time can be improved up to 4 times with a single unit GPU. Furthermore, with multi-unit GPU systems and faster deep-learning based remonstration algorithm, it becomes realistic to achieve implementation within milliseconds[41–44]. Here deep learning also helps with handling low light samples to produce super resolution in images; hence, low intensity samples may benefit from its appropriate implementation[42]. Information on the clinical translation of the SSIE's prototypic model developed in this study can be found in the Supplementary information. The direction of a faster SSIE with deep learning, SLM and optimized software will be explored in our near following future efforts along with its clinical translation to imaging animal or human subjects.

Conclusion

In summary, this study highlights the design, performance, and capabilities of SSIE, an inexpensive and reusable add-on system that surpasses endoscopic diffraction limits to produce high-resolution images with wide FOV and DOF. The SSIE can be easily integrated into standard white-light endoscopy (WLE) to non-invasively achieve micron-level resolution of surface features, surpassing the current systemic limitations. This capability can be helpful for screening and visualizing suspected lesions or anomalies using appropriate fluorescent dyes. Due to its wide FOV, the SSIE can be incorporated into standard endoscopes to capture images of the entire sample area. This is particularly beneficial for studying cases of GI infectious diseases or surface varices, which often spread across a wide FOV and DOF. Future advancements, such as the development of a high-speed

version of SSIE and the automation of image processing, may enable real-time surveillance of the GI tract. This could assist endoscopists in efficiently screening mucosa for potential abnormalities with optimal imaging metrics. Moreover, the imaging approach explored in this study may offer a new paradigm for studying the specificity of GI-based disorders such as Barrett's neoplasia or varices, which often involve a wide surface area that can be examined at high resolution. The design of the SSIE add-on allows for easy incorporation as a sleeve around both flexible and rigid endoscopes, regardless of whether they are high definition or intended for industrial or clinical use. Its simplicity makes it feasible to apply in medical and industrial fields, including endoscopy.

Materials

The experimental demonstration of the SSIE involved capturing 150 frames at a rate of 1 frame per second to generate the data shown in Fig. 5 and Fig. 6. The fluorescent signal was collected by the endoscopic lens using a long pass filter (580/40 nm). The reconstruction of wide-field-of-view images took approximately two to three minutes on a desktop computer equipped with a GTX 1080Ti graphics card and an i7-8700K processor. For the experiments, Rhodamine 6G dye at a concentration of 10 mg/mL mixed with a 10% glycerol solution was used. The dye was applied to the phantom by drop-casting it and drawing it using a fine needle tip to mimic features resembling fine vessel structures. Note, the Olympus CV-160 system has a poor image acquisition capabilities due to it being an older scope model. Hence, the imaging was conducted using the Teslong borescope endoscope due to its superior detector capabilities compared to the older CV-160 endoscope system (refer to the

Table 3 | Materials used in the add-on for the laboratory prototype.

Parts	Specifications
Sleeve/Add-on (To hold fiber)	Grey Pro (Standard resin: Incept)
Adhesive (Cyanoacrylate)	Loctite 4851 and Super Glue (Henkel, Gorilla)
Fiber (Multimode)	Multimode FG050UGA (Thorlabs) (0.22*NA*, High-OH, 50 µm core, Lambda: 250–1200 nm, FC/APC termination)
Medical grade TPU Film (Cover)	Polyether TPU (Polyzen)
Heat shrink (External binding)	Ultra-thin wall polyolefin heat shrink tubing (Buy heat shrink)
Film tape (To secure the fiber)	Polyimide film tape

Table 4 | Other components used for the SSIE system.

Materials	Specifications
Scope	CV-160 Olympus, Teslong's borescope endoscope system
Filter	Long pass 580/40 nm (Thorlabs)
Frame grabber	Epiphan VGA2USB device
Computer	GTX 1080Ti graphics card and a i7-8700K
Fluorescent dye	Rhodamine 6G (10 mg/mL)
Solution	10% glycerol
Mirrors	Optical mirrors (Thorlabs)
Fiber beam splitter	50/50 split ratio (Oz optics)
Free space beam splitter	50/50 split ratio (Thorlabs)
Collimators	Fiber collimators (Thorlabs)
Laser	Continuous wave, 532 nm, power 200 mW (Newport) Continuous wave, Tunable laser (Thorlabs)
Optical breadboard	24 x 36 inches (Thorlabs)
Posts, screws, clamps, post holders	Thorlabs
Needle and pipette	Standard laboratory pipette Fine needle tips (0.15 mm: Luter)
Phantom	Silicon material composite pads (MJW surgical and dental) Acrylic pipe rigid round tubes (Meccanixity) Elastic binding bands (Hoyols) Coupler adapter (90°)

Supplementary information Section 8). Additionally, as indicated in Section *Design and fabrication of the add-on*, whether the scope's application is clinical or industrial, the designed prototype developed in this study is translatable to both flexible and rigid scopes to perform the unanimous operation of image acquisition. In order to establish the ground truth in Fig. 5, a Mitutoyo REL-4800 compound microscope was used. Potential materials for a futuristic clinical add-on can be found in the Supplementary information Sections 2, 3, and 7.

References

1. Meng HY. Chapter 8 - Oncology—Acquired. In Meng HY. *Self-Assessment Questions for Clinical Molecular Genetics* 431–508 (Elsevier, Amsterdam, 2019).
2. Seeff LC, Richards TB, Shapiro JA et al. How many endoscopies are performed for colorectal cancer screening? Results from CDC's survey of endoscopic capacity. *Gastroenterology* **127**, 1670–1677 (2004).
3. Sonnenberg A, Amorosi SL, Lacey MJ et al. Patterns of endoscopy in the United States: analysis of data from the centers for Medicare and Medicaid services and the national endoscopic database. *Gastrointest Endosc* **67**, 489–496 (2008).
4. Ruhl CE, Everhart JE. Indications and outcomes of gastrointestinal endoscopy. Accessed 24 January 2023. https://www.niddk.nih.gov/about-niddk/strategic-plans-reports/burden-of-digestive-diseases-in-united-states/indications-outcomes-gastrointestinal-endoscopy/.
5. Global gastrointestinal endoscopy market analysis and forecast, 2019–2028. Accessed 24 January 2023. https://www.marketstudyreport.com/reports/global-gastrointestinal-endoscopy-market-analysis-and-forecast-2019-2028.
6. Spaner SJ, Warnock GL. A brief history of endoscopy, laparoscopy, and laparoscopic surgery. *J Laparoendosc Adv Surg Tech A* **7**, 69–73 (1997).
7. Olympus endoscopes. Accessed 24 January 2023. https://www.olympus-global.com/technology/museum/endo/?page=technology_museum.
8. Image Quality Metrics. Oncology medical physics. Accessed 24 January 2023. https://oncologymedicalphysics.com/image-quality-metrics/.
9. Vleggaar FP, Siersema PD. Barrett's esophagus, reflux esophagitis, and eosinophilic esophagitis. *Gastrointest Endosc* **76**, 496–500 (2012).
10. Zachariah R, Rombaoa C, Samarasena J et al. The potential of deep learning for gastrointestinal endoscopy—a disruptive new technology. In Xing L, Giger ML, Min JK. *Artificial Intelligence in Medicine* 223–245 (Elsevier, Amsterdam, 2021).
11. Shukla R, Abidi WM, Richards-Kortum R et al. Endoscopic imaging: how far are we from real-time histology. *World J Gastrointest Endosc* **3**, 183–194 (2011).
12. Hur C, Yachimski PS. Screening for esophageal squamous cell carcinoma. In Chandrasekhara V, Elmunzer BJ, Khashab MA et al. *Clinical Gastrointestinal Endoscopy* 3rd ed 291–301. e2 (Elsevier, Amsterdam, 2019).
13. Kwon RS, Adler DG, Chand B et al. High-resolution and high-magnification endoscopes. *Gastrointest Endosc* **69**, 399–407 (2009).
14. Reddymasu SC, Sharma P. Advances in endoscopic imaging of the esophagus. *Gastroenterol Clin North Am* **37**, 763–774 (2008).
15. ASGE Technology Committee. Confocal laser endomicroscopy. *Gastrointest Endosc* **80**, 928–938 (2014).
16. Nelson DB, Block KP, Bosco JJ et al. High resolution and high-magnification endoscopy: September 2000. *Gastrointest Endosc* **52**, 864–866 (2000).
17. Eberl T, Jechart G, Probst A et al. Can an endocytoscope system (ECS) predict histology in neoplastic lesions. *Endoscopy* **39**, 497–501 (2007).
18. Inoue H, Kazawa T, Sato Y et al. In vivo observation of living cancer cells in the esophagus, stomach, and colon using catheter-type contact endoscope, "endo-cytoscopy system". *Gastrointest Endosc Clin N Am* **14**, 589–594 (2004).
19. Das A, Sivak MV, Chak A et al. High-resolution endoscopic imaging of the GI tract: a comparative study of optical coherence tomography versus high-frequency catheter probe EUS. *Gastrointest Endosc* **54**, 219–224 (2001).
20. Bhushan S, Richards-Kortum R, Anandasabapathy S. Progress and challenges of global high-resolution endoscopy. *Int Arch Intern Med* **4**, 024 (2020).
21. Abraham E, Zhou JX, Liu ZW. Speckle structured illumination endoscopy with enhanced resolution at wide field of view and depth of field. *Opto-Electron Adv* **6**, 220163 (2023).
22. Mudry E, Belkebir K, Girard J et al. Structured illumination microscopy using unknown speckle patterns. *Nat Photonics* **6**, 312–315 (2012).
23. Yeh LH, Chowdhury S, Waller L. Computational structured illumination for high-content fluorescence and phase microscopy. *Biomed Opt Express* **10**, 1978–1998 (2019).
24. Ponsetto JL, Wei FF, Liu ZW. Localized plasmon assisted structured illumination microscopy for wide-field high-speed dispersion-independent super resolution imaging. *Nanoscale* **6**, 5807–5812 (2014).
25. Dan D, Lei M, Yao BL et al. DMD-based LED-illumination super-resolution and optical sectioning microscopy. *Sci Rep* **3**, 1116 (2013).
26. Qian J, Lei M, Dan D et al. Full-color structured illumination optical sectioning microscopy. *Sci Rep* **5**, 14513 (2015).
27. Pagac M, Hajnys J, Ma QP et al. A review of vat photopolymerization technology: materials, applications, challenges, and future trends of 3D printing. *Polymers* **13**, 598 (2021).
28. Guttridge C, Shannon A, O'Sullivan A et al. Biocompatible 3D printing resins for medical applications: a review of marketed intended use, biocompatibility certification, and post-processing guidance. *Ann 3D Print Med* **5**, 100044 (2022).
29. Raymond J. Which TPU is for you? Accessed 24 January 2023. https://www.bixbyintl.com/blog/which-tpu-is-for-you/.
30. Polyurethane film for medical industry. Accessed 24 January 2023. https://www.americanpolyfilm.com/medical-grade-tpu-film/.
31. PSI. Polyolefins are Everywhere. Accessed 24 January 2023. https://www.polymersolutions.com/blog/top-types-of-polyolefins-the-most-common-kind-of-plastics/.
32. Gumargalieva KZ, Zaikov GE, Polishchuk AY et al. Biocompatibility and biodegradation of polyolefins. *Int Polym Sci Technol* **29**, 60–72 (2002).
33. Burkhardt F, Schirmeister CG, Wesemann C et al. Pandemic-

driven development of a medical-grade, economic and decentralized applicable polyolefin filament for additive fused filament fabrication. *Molecules* **25**, 5929 (2020).
34. Hochberger J, Meves V, Ginsberg GG. Difficult cannulation and sphincterotomy. In Chandrasekhara V, Elmunzer BJ, Khashab MA et al. *Clinical Gastrointestinal Endoscopy* 3rd ed 563–570. e2 (Elsevier, Amsterdam, 2019).
35. Lee YU, Zhao JX, Ma Q et al. Metamaterial assisted illumination nanoscopy via random super-resolution speckles. *Nat Commun* **12**, 1559 (2021).
36. Lee YU, Posner C, Niev ZY et al. Organic hyperbolic material assisted illumination nanoscopy (Adv. Sci. 22/2021). *Adv Sci* **8**, 2170149 (2021).
37. Rex DK, Repici A, Gross SA et al. High-definition colonoscopy versus Endocuff versus EndoRings versus full-spectrum endoscopy for adenoma detection at colonoscopy: a multicenter randomized trial. *Gastrointest Endosc* **88**, 335–344.e2 (2018).
38. Schouw HM, Huisman LA, Janssen YF et al. Targeted optical fluorescence imaging: a meta-narrative review and future perspectives. *Eur J Nucl Med Mol Imaging* **48**, 4272–4292 (2021).
39. Chien FC. Simulation approach to optimize fluorescence imaging performance of wide-field temporal-focusing microscopy with tunable wavelength excitation. *Proc SPIE* **11076**, 110761Q (2019).
40. Kiepas A, Voorand E, Mubaid F et al. Optimizing live-cell fluorescence imaging conditions to minimize phototoxicity. *J Cell Sci* **133**, jcs242834 (2020).
41. Liao JH, Zhang CS, Xu XC et al. Deep-MSIM: fast image reconstruction with deep learning in multifocal structured illumination microscopy. *Adv Sci* **10**, 2300947 (2023).
42. Jin LH, Liu B, Zhao FQ et al. Deep learning enables structured illumination microscopy with low light levels and enhanced speed. *Nat Commun* **11**, 1934 (2020).
43. Shah ZH, Müller M, Wang TC et al. Deep learning based denoising and reconstruction of super-resolution structured illumination microscopy images. *Photonics Res* **9**, B168–B181 (2021).
44. Ling C, Zhang CL, Wang MQ et al. Fast structured illumination microscopy via deep learning. *Photonics Res* **8**, 1350–1359 (2020).

Acknowledgements

The authors would like to acknowledge Dr. Samuel Marcus for useful discussions.

Author contributions

E Abraham and ZW Liu produced the idea. E Abraham did the experiments. E Abraham prepared the figures. E Abraham prepared the paper. ZW Liu supervised the overall project.

Competing interests

The authors declare no competing financial interests.

Supplementary information

Supplementary information for this paper is available at https://doi.org/10.29026/oes.2025.240022